Double-Layer Cross-Coupled Silicon Nitride Multi-Ring Resonator Systems

J. Pan, S. Zhai, J. Feng, M. Shi, L. Zhou, G. Cong, R. Akimoto, and H. Zeng

***Abstract*— We demonstrate a double-layer Si_3N_4 multi-ring resonator system, where an *S*-bend waveguide is cross-coupled with a ring cavity loaded with two sub-ring resonators. The device performance is analyzed by using the transfer matrix method. The alignment-error-induced device performance variations are also discussed. The measured spectra coincide well with the simulated results. The device has high tuning flexibility and more design freedom with two sub-rings placed above the ring cavity. The spectrum profile can also be tuned by changing the cross-coupling coefficient. A heater placed above the resonator can shift the resonant wavelength effectively.**

***Index Terms*— Optical resonance, integrated optics, silicon nitride.**

I. Introduction

OPTICAL filters are a key component for dense wavelength-division-multiplexing (DWDM), which is widely used in optical communications and microwave photonics to increase the channel capacity [1], [2]. Optical filters can be based on interferometers such as Michelson-Gires-Tournois interferometers [3], Mach-Zehnder interferomet-ers (MZIs) [4], Sagnac interferometers [5], micro-cavity resonators [6] and arrayed-waveguide gratings [7].

For various integrated optical filter platforms, silicon nitride (Si_3N_4) is an ideal material as it has a wide transparency window and negligible nonlinear (two-photon) absorption losses [8]. The fabrication process of Si_3N_4 waveguides is compatible with complementary metal-oxide-semiconductor (CMOS) [9], which can also realize a three-dimensional (3D) vertical integration [10]. The 3D integration can provide a high fabrication tolerance and a compact size. A 3D resonator system with a bottom-layer microring cross-coupled to an *S*-bend waveguide on the top layer has been demonstrated [11]. The output spectrum profile can be designed by varying the coupling coefficient between the waveguide and the microring. The principle is similar to the Sagnac effect of a self-coupled device [2]. A planar cross-ring resonator MZI interleaver was also reported [12], but the crossing waveguide could cause additional insertion losses. For the self-coupled structure, the fabrication tolerance of the device can be improved [13], [14]. A dual-layer cross-coupled Si_3N_4 resonator with a sub-microring on the top layer has been proposed and demonstrated [15]. The resonant wavelength can be tuned by a micro-heater positioned above the feedback waveguide. It can provide more design freedom and fine-tuning of the spectrum.

For such a complex 3D integrated resonator, alignment errors may usually happen, which will cause the device performance to change. The detailed influence has not been studied. Besides, the dependence of the spectrum profile on the vertical coupling coefficient still needs further investigations. Thus, an alternative configuration of a 3D three-ring system is designed here. An S-bend waveguide is coupled with a racetrack ring cavity, which is loaded with two sub-ring resonators placed symmetrically on both sides of the waveguide. The racetrack ring is on the bottom layer. The S-bend and two sub-ring resonators are on the top layer. More rings can increase the design freedom and improve the spectrum tuning effect. The lightwave could resonate between the top and bottom layers multiple times and there are six waveguide coupling coefficients can be used. The device performance such as the extinction ratio and the passband can be tuned with varying the coupling coefficients.

II. Device Design

Fig. 1(a) presents a schematic of the double layer self-coupled multi-ring resonator filter, which comprises with an *S*-bend waveguide cross-coupled racetrack resonator system, with half of the resonator [*cmp*1 and *cmp*2 in Fig.1(a)] replaced by *U*-bend cross-coupled structures as in [16]. Fig. 1(b) shows the microscope image of the fabricated device. The waveguide has a height and width of 200 nm and 1.5 μm, respectively. It is essentially also a dual-layer cross-coupled structure with two sub-rings, where the racetrack resonator is on the bottom layer (Green part) and the two sub-rings together with the *S*-bend waveguide are on the top layer (Blue part). Two heaters are placed above the structure (Yellow part). The coupling length between the *S*-bend waveguide or the sub-rings and the racetrack resonator is denoted as L_{c1} or L_{c2}, respectively. The input light can propagate in clockwise or counterclockwise direction. The first light pathway

Manuscript received September 12, 2019; revised January 15, 2020; accepted January 16, 2020. Date of publication January 21, 2020; date of current version February 4, 2020. This work was supported in part by the National Natural Science Foundation of China under Grant 11774235, Grant 61705130, Grant 11727812, and Grant 11933005, in part by the Natural Science Foundation of Shanghai under Grant 17ZR1443400, in part by the Shanghai Rising-Star Program under Grant 19QA1406100, and in part by the Program for Professor of Special Appointment (Eastern Scholar) at Shanghai Institutions of Higher Learning. *(J. Pan and S. Zhai contribute equally to this letter.) (Corresponding author: J. Feng.)*

J. Pan, S. Zhai, J. Feng, and M. Shi are with the Shanghai Key Laboratory of Modern Optical System, Engineering Research Center of Optical Instrument and System (Ministry of Education), School of Optical-Electrical and Computer Engineering, University of Shanghai for Science and Technology, Shanghai 200093, China (e-mail: fjijun@usst.edu.cn).

L. Zhou is with the State Key Laboratory of Advanced Optical Communication Systems and Networks, Department of Electronic Engineering, Shanghai Institute for Advanced Communication and Data Science, Shanghai Jiao Tong University, Shanghai 200240, China.

G. Cong and R. Akimoto are with the Electronics and Photonics Research Institute, National Institute of Advanced Industrial Science and Technology (AIST), Tsukuba 305-8568, Japan (e-mail: r-akimoto @aist.go.jp).

H. Zeng is with the State Key Laboratory of Precision Spectroscopy, East China Normal University, Shanghai 200062, China, and also with the Jinan Institute of Quantum Technology, Shandong 250101, China.

Color versions of one or more of the figures in this letter are available online at http://ieeexplore.ieee.org.

Digital Object Identifier 10.1109/LPT.2020.2968291

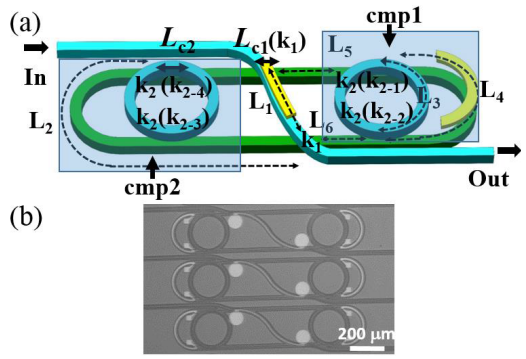

Fig. 1. (a) Schematic of a double-layer self-coupled multi-ring resonator system. (b) A microscope image of the fabricated devices.

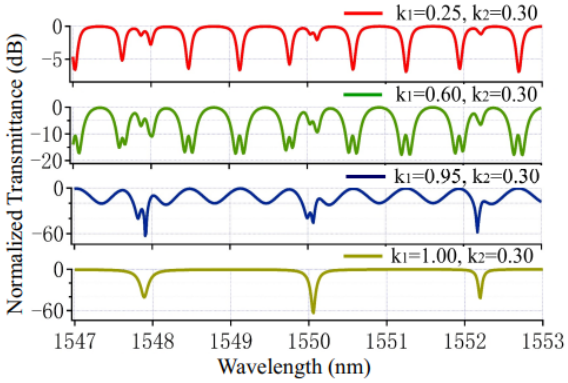

Fig. 2. Modeled device transmission spectra with a varying k_1 and a fixed k_2.

is through the waveguide directly, that is from the input-port to the S-bend waveguide and then to the output-port. Another pathway is the light coupling from the waveguide at the input-port to the bottom resonator. Then the light in the resonator propagates in clockwise direction and couples into the S-bend waveguide, then the light passes through the waveguide and into the resonator again and propagates in counterclockwise direction. There is a fixed path difference between the two pathways.

The device transmittance can be analyzed by using the transfer matrix method. The transmission and cross-coupling coefficients are t_1, k_1 or t_2, k_2 between the bottom resonator and the S-bend waveguide or the sub-rings ($k_1^2 + t_1^2 = 1$, $k_2^2 + t_2^2 = 1$ for lossless couplings). The transmittance t_0 is for the case without sub-rings, with the transmittance t_{AB} for a U-bend feedback-waveguide cross-coupled resonator, which is similar to that in [15], as in Eqs. (1) and (2). The transmittance of the left or right racetrack resonator system is indicated by t_{cmp1} or t_{cmp2}. The transmittance t_{s} of the multi-ring resonator can be obtained by substituting t_{cmp1} and t_{cmp2} with t_{AB} in Eq. (1).

$$t_0 = e^{-i\theta_1} \cdot \left[t_1^2 + \frac{2k_1^2 t_1^2 - k_1^4}{1 + t_1^2 t_{cmp1} t_{cmp2}} t_{cmp1} t_{cmp2} + \frac{2k_1^4 t_1^2 (t_{cmp1} t_{cmp2})^2}{(1 + t_1^2 t_{cmp1} t_{cmp2})^2} \right], \tag{1}$$

$$t_{AB} = \frac{k_2^2 e^{-i\theta_3} - t_2^2 e^{-i\theta_4} + e^{-i(2\theta_3 + \theta_4)}}{1 + k_2^2 e^{-i(\theta_3 + \theta_4)} - t_2^2 e^{-i2\theta_3}} e^{-i(\theta_5 + \theta_6)}, \tag{2}$$

$$t_s = e^{-i\theta_1} \cdot \left[t_1^2 + \frac{2k_1^2 t_1^2 - k_1^4}{1 + t_1^2 t_{AB} t_{AB}} t_{AB} t_{AB} + \frac{2k_1^4 t_1^2 (t_{AB} t_{AB})^2}{(1 + t_1^2 t_{AB} t_{AB})^2} \right]. \tag{3}$$

Here, θ_{i} ($i = 1, 2, \ldots, 6$) represents the accumulated phase shift in a waveguide with a length of L_{i}.

Various spectral profiles can be realized with varying k_1 as shown in Fig. 2, with $k_1 = 0.25$, 0.60, 0.95 and 1 while $k_2 = 0.3$ at the transverse electric (TE) polarization. The device geometric parameters are $L_1 = 390\ \mu$m, $L_2 = (532 + 100\pi)\ \mu$m, $L_3 = 100\pi\ \mu$m, $L_4 = (100 + 100\pi)\ \mu$m, $L_5 = 141\ \mu$m and $L_6 = 391\ \mu$m, as shown in Fig. 1(a). The waveguide propagation loss is about 1.3 dB/cm, obtained by the cutback method. The corresponding extinction ratios are 7.2 dB, 13.2 dB, 31.49 dB and 70.3 dB near 1550-nm wavelength, which increase with k_1. The electromagnetically induced transparency (EIT)-like [17], [18] resonance feature depends on k_1. The EIT-like resonance is absent with $k_1 = 1$. The resonance dip splits into an EIT-like spectrum at 1549.8 nm, which becomes a new oscillation and disappears with the increased k_1. A quality (Q) factor of 2.0×10^4 is obtained with $k_1 = 0.25$ at a wavelength of 1549.8 nm, which is calculated by the ratio of the resonant wavelength to the half-width of the crest. For the split resonance dip, the Q-value can be roughly obtained with a Lorentzian-fitting of the whole dip. The Q-value is limited by the multi-coupling system and the high waveguide propagation loss originated from the material absorption and the microring bending loss due to a thin waveguide layer. For the full-coupling case ($k_1 = 1$), the structure is turned into the case of having the two U-bend waveguides coupled. Resonance features are similar to those in Ref. [16], which have a free spectral range (FSR) of 2.13 nm. Only one path exists for the device due to the unity coupling coefficient.

Fig. 3(a) reveals the influence of k_2 on the transmission spectrum, where k_1 is fixed at 0.25 with $k_2 = 0.25$, 0.50, 0.75 and 1. The dense notch filtering performance can be controlled, showing potential applications in DWDM systems. The extinction ratio slightly changes with k_2 at new resonance positions. It seems that k_1 mainly determines the filtering profile while small resonance shifts and extinction ratio changes can be influenced by k_2. This may be due to that the main resonant filtering feature is caused by the interference between clockwise and counterclockwise propagating light in the resonator, which is determined by k_1. Meanwhile, the performance of the U-bend feedback-waveguide cross-coupled resonator can be tuned by k_2, which causes some fine-tuning to the spectrum. However, for the case when $k_2 = 1$ or 0, the structure is reduced to a simple S-bend waveguide-coupled ring resonator. The resonance characteristics are similar to those in [11].

Compared with the film-thickness-induced coupling coefficient variation, alignment errors usually happen during a multi-layer device fabrication and may cause a moderate performance change due to the waveguide displacement and an asymmetry in the coupling coefficents between the bottom resonator and the top sub-rings, which are denoted as k_{2-1}, k_{2-2}, k_{2-3} and k_{2-4} instead of k_2, as shown in Fig. 1(a). The simulated results with $k_1 = 0.60$ are shown in Fig. 3(b).

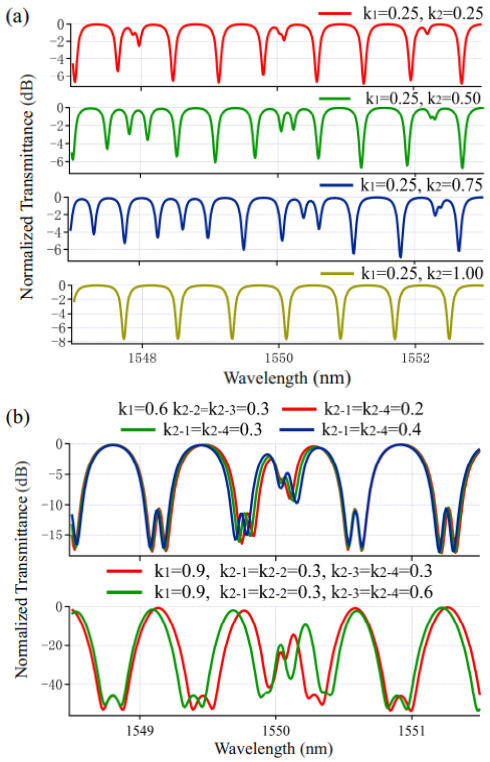

Fig. 3. Modeled transmission spectra for the device with a varying k_2 and a fixed k_1. (b) Modeled transmission spectra for the filter with an asymmetry in the coupling coefficents between the bottom resonator and the top sub-rings.

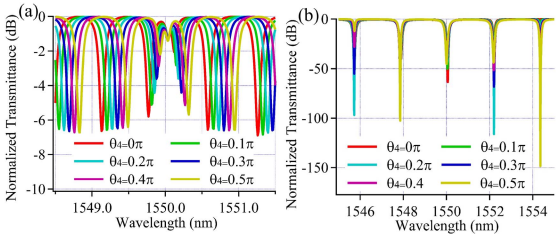

Fig. 4. Modeled transmission spectrum evolution with an additional phase shift (from 0 to 0.5π) is applied to the racetrack resonator with the coupling coefficients of (a) $k_1 = 0.25$, $k_2 = 0.30$ and (b) $k_1 = 1$, $k_2 = 0.30$.

The cross-coupling coefficients k_{2-2} and k_{2-3} are chosen to be 0.3 while k_{2-1} and k_{2-4} are 0.2, 0.3 and 0.4. A slight resonant-wavelength-shift of 0.03 nm happens, which can provide a high fabrication tolerance for alignment errors. For varying the sub-ring coupling coefficient with $k_{2-1} = k_{2-2} = 0.3$, k_{2-3} and k_{2-4} are 0.3 or 0.6 for comparison. It can be seen that the main profiles are similar but the resonance position (around 1550 nm) changes with a wavelength shift of 0.08 nm.

Fig. 4(a) shows the spectrum change with phase θ_4, corresponding to a phase shift applied to the bottom racetrack resonator. The coupling coefficients are fixed at $k_1 = 0.25$ and $k_2 = 0.30$. The phase tuning to θ_4 can result in an effective change of the resonant wavelength. A 0.075-nm resonant wavelength shift is observed for a 0.1π phase change at the resonant wavelength of 1549.5 nm. There are no resonant wavelength shifts at a wavelength of 1550 nm, where the EIT-like resonance profile happens. For $k_1 = 1$, the resonant wavelength has little shifts, as shown in Fig. 4(b). A phase-shift only varies the extinction ratio of the resonance dip while each resonance wavelength has a different behavior, since the corresponding group index and thus the static optical phase are different. Moreover, additional phase shifts on the *S*-bend waveguide do not change the spectrum profile, which is similar to that shown in [11] and is not shown here for simplicity.

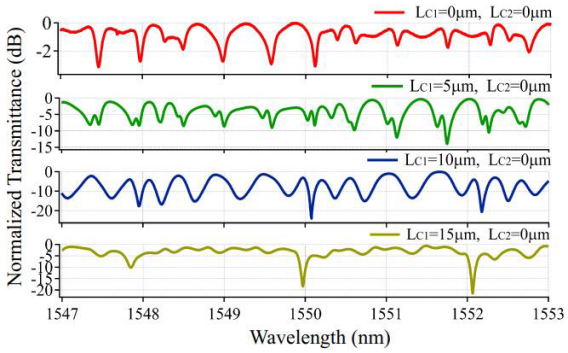

Fig. 5. Measured transmission spectra for the device with a coupling length L_{c1} of 0, 5, 10 and 15 μm, respectively.

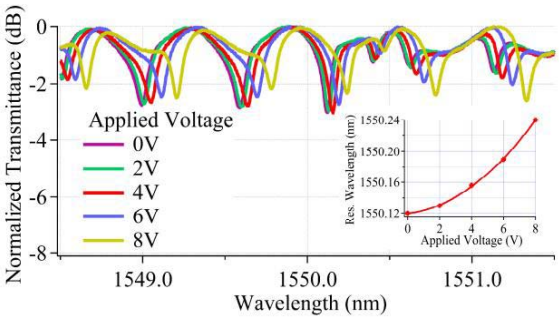

Fig. 6. Active tuning of the device transmission spectrum by the heater above the racetrack resonator for $L_{c1} = 0$ and $L_{c2} = 0$ μm. Inset: resonant wavelength with the applied voltage.

III. Performance and Discussion

The device fabrication is similar to that in [16]. The fabricated device has a footprint of 1.2×0.3 mm^2. The measurement setup incorporates an amplified spontaneous emission (ASE) source, a polarizer for adjusting the light polarization state, an input objective lens, an output tapered fiber and an optical spectrum analyzer (OSA). Fig. 5 shows the measured transmission spectra of the device with coupling lengths $L_{c1} =$ 0 μm, 5 μm, 10 μm, 15 μm and $L_{c2} = 0$ μm, which are normalized with the maximum transmittance. The k_1 is calculated to be about 0.25, 0.60, 0.95 and 1, respectively. The zero-coupling length means that there are no straight coupling sections, but coupling still occurs due to the dual-layer crossed waveguides. The k_1 for $L_{c2} = 0$ μm is about 0.30. At $L_{c1} = 0$ μm, a Q factor of 2.0×10^4 can be realized. The measured spectra agree well with the simulation results as shown in Fig. 2, which have a similar spectral profile and a similar filtering performance. The extinction ratios are about 3.2 dB, 5.6 dB, 21.3 dB and 17.3 dB near 1550 nm for different coupling lengths. The resonance dip has a small blue-shift near 1550 nm for the coupling length of 15 μm, which may be caused by the slightly unbalanced coupling coefficients between the top sub-ring or the waveguide and the bottom resonator as in the simulation in Fig. 3(b).

Fig. 6 shows the spectrum tuning with a voltage applied to the heater above the racetrack resonator, with both the coupling lengths L_{c1} and L_{c2} of 0 μm. The resonant wavelength has

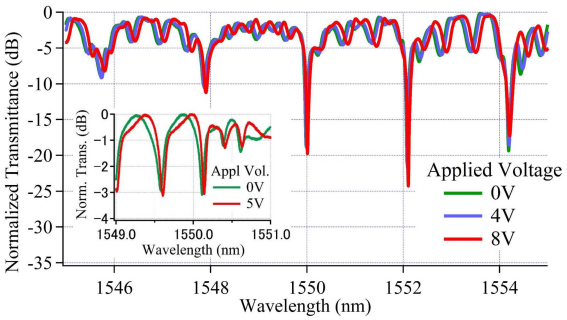

Fig. 7. Resonant spectrum changes by the heater above the racetrack resonator with $L_{c1} = 15$ and $L_{c2} = 0$ μm. Inset: spectrum change by the heater above the S-bend waveguide.

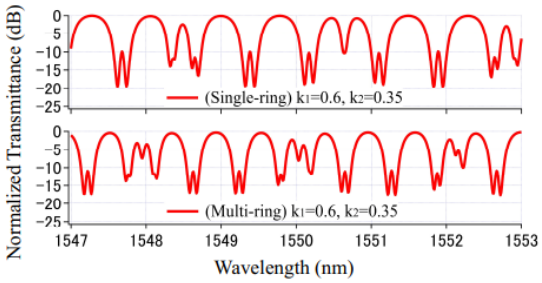

Fig. 8. Comparison of transmission spectra of the single sub-ring and dual sub-ring resonator systems with $k_1 = 0.6$, $k_2 = 0.35$.

a red-shift when the voltage increases. With an 8-V voltage applied to the heater, a 0.12-nm shift can be obtained. Inset of Fig. 6 shows the resonant wavelength change, which has a quadratic relationship with the applied voltage (as the fitted solid line) since the waveguide effective index changes almost linearly with the generated heat. The thermal tuning efficiency is not so high mainly due to the low thermal coefficient of Si_3N_4 material, which is about 2.45×10^{-5} RIU/° [19]. The large vertical coupling gap spacing and the thick cladding layer between the heater and the waveguide also decrease the thermal tuning efficiency.

Fig. 7 shows the transmission spectra when the voltage is applied to the heater above the racetrack resonator with $L_{c1} = 15$ μm. The resonant wavelength is almost fixed and only the extinction ratio varies. It is consistent with the simulated results in Fig. 4(b). There are small oscillations in the transmission spectra, which may be caused by light multiple reflections between the waveguide input/output facets. Inset of Fig. 7 shows the spectrum change when the voltage is applied to the heater above the S-bend waveguide. There are no obvious resonant wavelength shifts, since the resonant wavelength is independent of the phase of the S-bend waveguide. The slight difference in the spectrum may be due to the cross-coupling coefficient change caused by the thermal crosstalk.

Fig. 8 shows the simulated spectra for the single sub-ring and dual sub-ring cases with the same coupling coefficients. The dual sub-ring structure has a more complex filtering spectrum. Every two main crests, there is one split crest and then one tiny crest is followed by two crests for the single-ring case. The spectral profile can be effectively tuned as shown in Figs. 2 and 3(a). The multi-ring system can provide a high sensitivity, a compact structure and a high fabrication tolerance. Besides, the coupling coefficients between the top sub-ring and the bottom resonator can be different, which gives more design freedom to satisfy various filtering applications.

IV. Conclusion

To summarize, we demonstrated a 3D integrated system consisting of a racetrack resonator coupled with an S-bend waveguide and two sub-microrings. Different spectral profiles are obtained by varying the coupling coefficients. The alignment-error-caused vertical asymmetric coupling coefficients between the resonator and the sub-rings cause the resonance position changes. The 3D integrated device can provide a compact footprint and a larger fabrication tolerance compared with conventional planar structures. The multi-ring system also shows a potential of building complex filtering or multifunction systems, which is expected to have a wide application prospect beyond optical communications.

References

[1] X. P. Li, K. X. Chen, and L. F. Wang, "Compact and electro-optic tunable interleaver in lithium niobate thin film," *Opt. Lett.*, vol. 43, no. 15, p. 3610, Aug. 2018.
[2] S. Lai, Z. Xu, B. Liu, and J. Wu, "Compact silicon photonic interleaver based on a self-coupled optical waveguide," *Appl. Opt.*, vol. 55, no. 27, p. 7550, Sep. 2016.
[3] C.-H. Hsieh *et al.*, "Flat-top interleavers using two Gires-Tournois etalons as phase-dispersive mirrors in a Michelson interferometer," *IEEE Photon. Technol. Lett.*, vol. 15, no. 2, pp. 242–244, Feb. 2003.
[4] L. Luo *et al.*, "High bandwidth on-chip silicon photonic interleaver," *Opt. Express*, vol. 18, no. 22, pp. 23080–23087, Aug. 2010.
[5] J. Capmany, P. Muñoz, S. Sales, D. Pastor, B. Ortega, and A. Martinez, "Arrayed waveguide Sagnac interferometer," *Opt. Lett.*, vol. 28, no. 3, p. 197, Feb. 2003.
[6] E. Shah Hosseini, S. Yegnanarayanan, A. H. Atabaki, M. Soltani, and A. Adibi, "High quality planar silicon nitride microdisk resonators for integrated photonics in the visible wavelength range," *Opt. Express*, vol. 17, no. 17, p. 14543, Aug. 2009.
[7] B. I. Akca and C. R. Doerr, "Interleaved silicon nitride AWG spectrometers," *IEEE Photon. Technol. Lett.*, vol. 31, no. 1, pp. 90–93, Jan. 1, 2019.
[8] D. J. Moss, R. Morandotti, A. L. Gaeta, and M. Lipson, "New CMOS-compatible platforms based on silicon nitride and Hydex for nonlinear optics," *Nature Photon.*, vol. 7, no. 8, pp. 597–607, Aug. 2013.
[9] J. Feng and R. Akimoto, "Silicon nitride polarizing beam splitter with potential application for intersubband-transition-based all-optical gate device," *Jpn. J. Appl. Phys.*, vol. 54, no. 4S, Apr. 2015, Art. no. 04DG08.
[10] J. Feng and R. Akimoto, "Vertically coupled silicon nitride microdisk resonant filters," *IEEE Photon. Technol. Lett.*, vol. 26, no. 23, pp. 2391–2394, Dec. 1, 2014.
[11] S. Zhai, J. Feng, X. Sun, R. Akimoto, and H. Zeng, "Vertically integrated waveguide self-coupled resonator based tunable optical filter," *Opt. Lett.*, vol. 43, no. 15, p. 3766, Aug. 2018.
[12] J. Song *et al.*, "Effective thermo-optical enhanced cross-ring resonator MZI interleavers on SOI," *Opt. Express*, vol. 16, no. 26, p. 21476, Dec. 2008.
[13] Z. Zou *et al.*, "Tunable two-stage self-coupled optical waveguide resonators," *Opt. Lett.*, vol. 38, no. 8, p. 1215, Apr. 2013.
[14] L. Zhou, T. Ye, and J. Chen, "Coherent interference induced transparency in self-coupled optical waveguide-based resonators," *Opt. Lett.*, vol. 36, no. 1, p. 13, Jan. 2011.
[15] S. Zhai *et al.*, "Dual-layer cross-coupled tunable resonator system in a three-dimensional Si_3N_4 photonic integration platform," *J. Lightw. Technol.*, vol. 37, no. 13, pp. 3298–3304, Jul. 1, 2019.
[16] J. Feng, R. Akimoto, Q. Hao, and H. Zeng, "Three-dimensional cross-coupled silicon nitride racetrack resonator-based tunable optical filter," *IEEE Photon. Technol. Lett.*, vol. 29, no. 9, pp. 771–774, May 1, 2017.
[17] X. Zhou, T. Zhang, X. Yin, L. Chen, and X. Li, "Dynamically tunable electromagnetically induced transparency in graphene-based coupled micro-ring resonators," *IEEE Photon. J.*, vol. 9, no. 2, pp. 1–9, Apr. 2017.
[18] Z. Zhang *et al.*, "Electromagnetically induced transparency-like effect in microring-Bragg gratings based coupling resonant system," *Opt. Express*, vol. 24, no. 22, p. 25665, Oct. 2016.
[19] A. Arbabi and L. L. Goddard, "Measurements of the refractive indices and thermo-optic coefficients of Si_3N_4 and SiO_x using microring resonances," *Opt. Lett.*, vol. 38, no. 19, p. 3878, Oct. 2013.